PEOPLE's DEMOCRATIC REPUBLIC OF ALGERIA

MINISTRY OF HIGHER EDUCATION AND SCIENTIFIC RESEARCH

UNIVERCITY OF MEDEA

FACULTY OF TECHNOLOGY



Presented to obtain the Master's degree in Mechanical Engineering

Specialty: renewable energies in mechanics

By:

Merrah Dounya

Thesis:

AN IN-DEPTH INVESTIGATION OF THE COMBINED OPTOELECTRONIC AND PHOTOVOLTAIC PROPERTIES OF LEED-FREE PEROVSKITE SOLAR CELLS USING DFT AND SCAPS-1D FARMEWORKS.

Directed by:

Dr. RABHI Selma

Dr. CHABA MOUNA Sarah

2023/2024

Acknowledgement

First of all Alhamdulillah ever and forever.

I would like to express my deepest gratitude to Dr Selma Rabhi and Dr Sarah Chaba Mouna, for their unwavering support, guidance, and encouragement throughout the duration of the research. Their expertise and insightful feedback have been invaluable in shaping the direction and outcome of this thesis.

I extend my heartfelt gratitude to the esteemed members of the jury Mr Alliche Mounir and Dr Tahar Souad for their time. Thank you for your invaluable contributions.

I would like to extend my appreciation to administrative staff, whose assistance and efficiency have facilitated my academic journey significantly.

A special thanks to my colleagues and friends, whose companionship and support made the challenging moments more manageable.

My heartfelt thanks go to my family for their unconditional love and encouragement. To my parents and my siblings, thank you for every things, your unwavering faith in my abilities and constant support have been my pillars of strength.

Lastly, I would like to acknowledge everyone I meet in my journey education.

Thank you all for making this thesis possible.

Dedication

"AND THEIR LAST PRAYERS IS ELHAMDULLILAH"

This thesis is lovingly dedicated

To my beloved family, whose unwavering support and encouragement have been my constant source of strength and love.

To my parents M. MILOUD and FERRAH KH, your sacrifices and belief in me have made this achievement possible.

To my brothers OMAR, RACHID and MOUSTAPHA, and my sisters FIFI, FATI, DJIMI and NINA, and my cousin AHLEM, your encouragement and love has been invaluable.

To Dr SELMA RABHI and Dr SARA CHABA MOUNA, your invaluable support and guidance have been instrumental in the completion of this work. Thank you both for your immense contributions. This work is a testament to your generosity and expertise.

To my special and beautiful friends IMANE, LAILA, NADOUCHA, MAROUA and all my friends from journey education, thank you for your love, your patience, and for always being there to lift my spirits. Your friendship has made this challenging journey not only bearable but truly memorable. This work is a testament to the power of friendship and the love we share.

With deepest gratitude and affection, I dedicate this thesis to you.

DOUNYA MERRAH

Abstract

In last years, ABX_3 halide perovskite materials have spread widely in the world of photovoltaic solar cells as absorbers layer, and this is what attracted the interest of many scientists for made it a subject of a lot of scientific research. In our work, we study the structural, electronic, elastic and optical properties of Sodium hexa-fluorosilicate $NaSiF_3$ utilizing Material Studio software based on density functional theory (DFT) calculations using CASTEP. The results obtained after studying the computed elastic and mechanical properties of the $NaSiF_3$ cubic structure indicate that this material possesses high mechanical stability. The optical properties reveal a strong absorption in the ultraviolet (UV) region. The electronic properties demonstrate that $NaSiF_3$ has indirect band gap semiconductor (R-Γ), making it appropriate for applications as photo-detectors. We have simulated also using SCAPS software the electronic behavior of $NaSiF_3$-based solar cell.

Keywords: Perovskite, $NaSiF_3$, CASTEP, density functional theory (DFT), SCAPS.

Résumé

Au cours des dernières années, les matériaux perovskite hologènes ABX_3 se sont largement répandus dans le monde des cellules solaires photovoltaïques comme couche d'absorbants, et c'est ce qui a attiré intérêt de nombreux scientifiques pour l'avoir fait l'objet de beaucoup de recherches scientifiques. Dans notre travail, nous étudions les propriétés structurelles, électroniques, élastiques et optiques de Sodium l'exa-fluorosilicate $NaSiF_3$ en utilisant le logiciel Materials Studio basé sur les calculs de la théorie fonctionnelle de la densité (DFT) utilisant CASTEP. Les résultats obtenus après l'étude des propriétés élastiques et mécaniques calculées de la structure cubique $NaSiF_3$ indiquent que ce matériau possède une stabilité mécanique élevée. Les propriétés optiques relèvent une forte absorption dans la région ultraviolette (UV). Les propriétés électroniques démentent que $NaSiF_3$ possède un semi-conducteur à bande interdite indirecte (R-Γ), ce qui le rend approprié pour des applications telles que les photo-détecteurs. Nous avons également simulé en utilisant le logiciel SCAPS le comportement optoélectronique de la cellule solaire à base de $NaSiF_3$.

Mots clés : Pérovskite, $NaSiF_3$, CASTEP, propiétés, (DFT), SCAPS.

الملخص

في السنوات الأخيرة، انتشرت مواد ABX_3 هاليد بيروفسكايت على نطاق واسع في عالم الخلايا الشمسية الكهروضوئية كطبقة ممتصة. وهذا ما جذب اهتمام العديد من العلماء لجعلها موضوع الكثير من الأبحاث العلمية. في عملنا، ندرس الخصائص الهيكلية، الإلكترونية ، المرونة والخصائص البصرية لفلورو سيليكات الصوديوم $NaSiF_3$ باستخدام برنامج Material studio على أساس حسابات نظرية الكثافة الوظيفية (DFT) باستخدام CASTEP. النتائج التي تم الحصول عليها بعد دراسة المرونة والخصائص الميكانيكية المحسوبة للهيكل المكعب تشير إلى أن هذه المادة تمتلك ثباتاً ميكانيكياً عالياً. تكشف الخصائص البصرية عن امتصاص قوي في منطقة الأشعة فوق البنفسجية. الخصائص الإلكترونية تثبت أن لديها فجوة نطاق غير مباشرة، مما يجعلها مناسبة لتطبيقات كاشفات الأشعة. لقد قمنا أيضا بمحاكاة السلوك الالكتروني للخلايا الشمسية باستخدام برنامجSCAPS .

الكلمات المفتاحية: بيروفسكايت ، $NaSiF_3$ ، CASTEP ، الخصائص ، (DFT) ، SCAPS .

Figures list

Figure 1. a) The first silicon cell ; b) The page of a note book of C. Fuller, witnessed by D. Chapin[1]. 4
Figure 2. Wafer-based solar technology[2].....5
Figure 3. CIGS Solar Cell composition[2].....7
Figure 4. Shows schematic diagram of TSC, (a) mechanically stacked 4T, (b) monolithically integrated 2T, and (c) optical splitting of the solar[4]. 8
Figure 5. (a) Typical J-V characteristics of a solar cell, in dark (black line) and under illumination (red line). The corresponding V_{OC} and J_{SC} are presented in the figure. **(b)** The output power of the cell (red line) as function of voltage. The MPP of the device is presented by a black dot in the figure. 9
Figure 6. Crystal structure of 3D cubic perovskite. Cation A is located in the void between the BX6 octahedra. In a crystal unit cell, A is located in the corners, B is in a body-centered position, and X is in a face-centered position[18]. 12
Figure 7. SCAPS-1D software startup control panel[32]. 19
Figure 8. SCAPS-1D solar cell definition panel with perovskite structure. 20
Figure 9. Panel for defining the physical properties of the layers. 21
Figure 10. Crystalline structure of $NaSiF_3$. 24
Figure 11. Electronic band structure of $NaSiF_3$. 25
Figure 12. Total and partial DOS of $NaSiF_3$. 26
Figure 13. Computed dielectric imaginary part ε2(ω) and dielectric real part ε1(ω) for the NaSiF3. 28
Figure 14. Computed refractive index η (ω). 29
Figure 15. Computed extinction coefficient k (ω).....30
Figure 16. Absorption coefficient for NaSiF3. 31
Figure 17. Reflectivity of NaSiF3 R (ω).....31
Figure 18. Energy-loss spectrum L (ω). 32
Figure 19. J-V curve of Se:Te/CuO_2/ $NaSiF_3$/ ZrS_2/ AZO. 33

Tables List

Table II-1:Parameters used for the simulation of the structure of solar cells in perovskite. ...22
Table III-1: Values of calculated elastic constants C_{ij}. 27
Table III-2: Photovoltaic parameters of Te/CuO_2/$NaSiF_3$/ZrS_2/AZO perovskite solar cell. ..32

Table of content

Acknowledgement
Dedication
Abstract
Résumé
الملخص
Figures list
Tables List
Table of content
List of abbreviations
General introduction 2
I.1 Introduction 4
I.2 Solar cells 4
I.3 Photovoltaic technologies 5
I.3.1 Wafer-based Solar Technology (First generation) 5
I.3.2 Thin Film Technology 6
I.3.3 Third Generation Solar Technologies 7
I.4 Performance characterization of solar cells 8
I.5 Perovskite solar cell 11
I.5.1 Structure of Perovskite 11
I.5.2 Structure of NaSiF3-based perovskite solar cell: 13
II Simulation of Perovskite solar cell 16
II.1 Introduction 16
II.2 BIOVIA Material Studio 16
II.2.1 CASTEP 16
II.3 Presentation of SCAPS-1D 18
II.3.1 Solar cell structure 21
III Results and discussions 24
III.1 DFT simulation 24
III.2 Crystalline structure 24
III.3 Band structure 25
III.4 Total and partial density of state 26

III.5 Elastic properties 27
III.6 Optical properties.....27
General Conclusion 34
References.....35

List of abbreviations

- 1D One-dimensional
- 3D Three-dimensional
- PVK Perovskite
- HTL Hole Transport Layer
- ETL Electron Transport Layer
- PCE Power Conversion Efficiency
- PV Photovoltaic
- SCs Solar Cells
- KAUST King Abdullah University of Science and Technology
- MPP Maximum Power Point
- HOMO Higher Occupied Molecular Orbital
- LUMO Lowest Unoccupied Molecular Orbital
- UV Ultraviolet
- CB Conduction Band
- VB Valence Band
- R&D Research And Development
- TCM Theory of Condensed Matter
- DFT Density Functional Theory
- GGA Generalized Gradient Approximation
- LDA Local Density Approximation
- QE Quantum Efficiency
- FF Filing Factor

GENERAL INTRODUCTION

General introduction

Pervskite solar cells are known in the photovoltaic world, since they have achieved high yields very quickly and using simple and inexpensive deposition methods. This rapid progress in a short time is an unprecedented phenomenon, which is revolutionizing solar cell research.

Since 2009, hybrid halogenated perovskite, and in particular the methylammonium lead iodide $CH_3NH_3PbI_3$, have established themselves as very promising absorbers for solar cells, demonstrating remarkable performances in a short time. But the solar cells based on lead methylammonium iodide suffer instability and degradation, its dimming leads to the diffusion of Pb and the latter is a toxic material that has a negative impact on the environment.

One of the promising solutions to overcome these problems is to find inorganic materials known by their performance on the stability of perovskite. $NaSiF_3$ is one of the materials that has not received as much research.

In this present work, a theorical study of the physical properties of $NaSiF_3$ will be made using a module called CASTEP which is located in the Material Studio softwere. In addition, the digital modeling of the solar cell based on 3D PVK, using SCAPS-1D will be done. Two inorganic materials such as will be used as hole transport layers (HTL): Se/Te, Cu_2O and ZrS_2 will be used as electron transport layers (ETL). So the perovskite solar cell based $NaSiF_3$ will be studied in this work.

This thesis is divided into three chapters, a chapter with general information on photovoltaic cells,in particular halogenated hybrid perovskite cells. The second chapter is devoted to the burial. This thesis is then concluded with a general conclusion.

Chapter I: Introduction to Perovskite-based solar cells

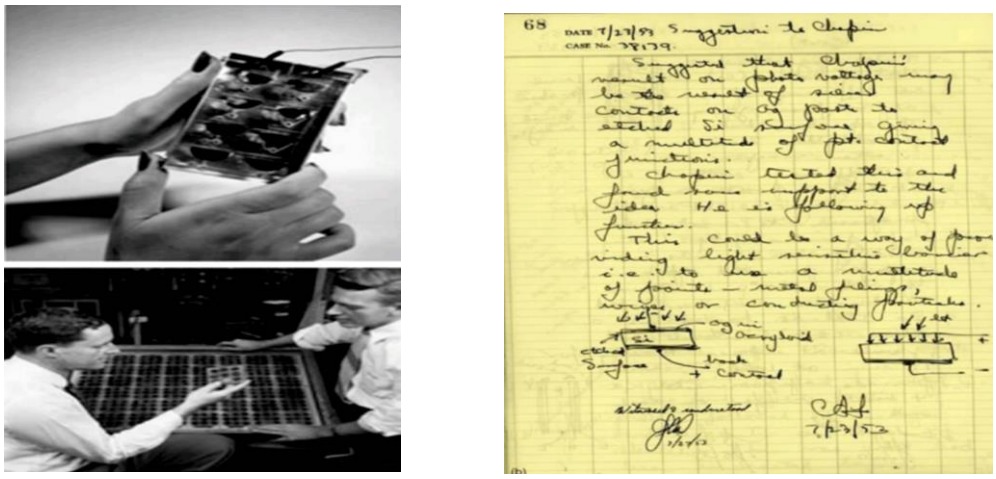
I Introduction to perovskite-based solar cells

I.1 Introduction

In this chapter, we will talk about solar cells, its different technologies, and performance characterization of a solar cell. Then, we will discuss about perovskite solar cell and the structure of $NaSiF_3$-based perovskite solar cell.

I.2 Solar cells

Solar cells, or photovoltaic cells, are devices designed to convert sunlight directly into electricity through the photovoltaic effect, this process involves the creation of voltage or electric current in a material when exposed to light. These devices are made of semiconducting materials, most commonly silicon. The photovoltaic effect has been discovered for the first time in Bell Laboratory in USA in 1954[1], where they could fabricate Si-based solar cell with PCE around 6%. It is based on the sun light, which absorbed by a semi-conductor material, where there is no light absorption happens when the energy of incoming light is below the band gap (also known as the absorption edge) of the semiconductor material used in solar cells. Photovoltaic are structured into a ‘p-n’ junction. The ‘p’ layer contains positive charges, and the ‘n’ layer has negative charges. When sunlight hits the cell, it knocks electrons loose from the atoms, and these electrons can be captured as electric current. In this structural arrangement, when a photon of sufficient energy strikes the p-type and n-type junction, an electron is ejected by gaining energy from the striking photon and moves from one layer to another. This creates electrons and holes in the process, generating electric power.



(a) (b)

Figure 1. a) The first silicon cell ; b) The page of a note book of C. Fuller, witnessed by D. Chapin[1].

I.3 Photovoltaic technologies

A solar cell is a device with the primary function of transforming light energy directly into electricity through photovoltaic effect. Its electrical characteristics which includes current, voltage, or resistance, differs with exposure to light energy from any source, whether natural or artificial. There are four generation of solar cell, in the next section we will describe each generation separately[2].

I.3.1 Wafer-based Solar Technology (First generation)

The first sector of photovoltaics to enter the market were the Silicon-based PV cells, they comprise more than 80% of the world's installed capacity and have a 90% market share. This generation Si-based cells comprises of crystalline silicon, example of which are poly-silicon and mono-crystalline silicon, and recently the GaAs is integrate in this field [2].

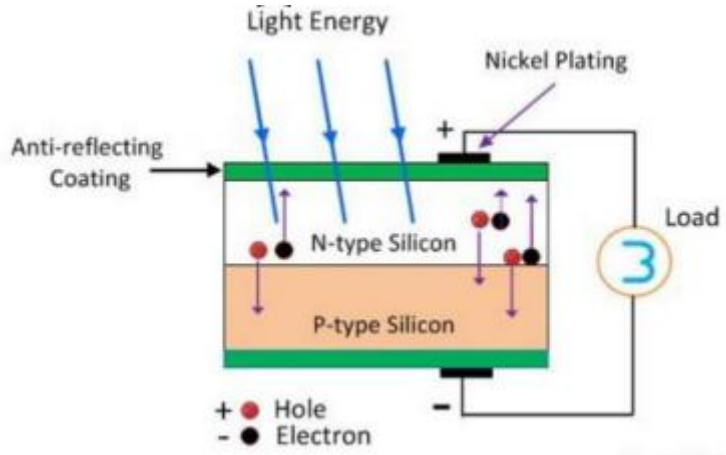


Figure 2. Wafer-based solar technology[2].

I.3.1.1 Mono-crystalline Solar Cell

Mono crystalline solar cell, are made using a single crystal of silicon (Si) by the Czochralski process. The production of the Si crystals is usually done with high accuracy, from large ingots. Mono-crystalline cells have been found to measure 26.1% in efficiency. However, a higher efficiency of 24.4% has been achieved from an enhanced multi-crystalline silicon solar cell, as well as a rise 26.1% for mono-crystalline cells. This multi-crystalline cells enhancement emanated from covering multi-crystalline surfaces with oxides formed thermally so as to limit their detrimental electronic processes and from isotropic etching, producing a hexagonally symmetric "honeycomb" surface texture[2].

K. E. Sarah, P. U. Ronald, and P.O.E.N.C presented a traditional technological activity through screen printed process of mono-crystalline silicon solar cells manufacture. Schottky and Zener diodes provided protection for the device while the cells were linked to the PV modules to produce electricity. The module found practical application in traffic lighting for pedestrian crossing[2].

I.3.1.2 Poly-crystalline Silicon Solar Cell (Poly-Si or McSi)

Polycrystalline PV modules are formed from various crystals, joined together in a unit cell. The forming procedure is cost effective, involving cooling a graphite mould composed of molten silicon [2].

I.3.2 Thin Film Technology

These represent the Second generation cells and are amorphous silicon, Cadmium Telluride (CdTe) and Copper Indium Gallium di-Selenide (CIGS) cells. They are commercially found and applied extensively in utility-scale photovoltaic power stations, as they have better performance under cloudy conditions[2].

I.3.2.1 Amorphous Silicon Solar Cell (A-Si)

This type of solar cell was the most commonly known amongst thin films, though it hasbeen on the market for over 15 years. It has been commonly utilized in pocket and desktop calculators, and more recently in solar panels for domestic and utility generation of electricity. Amorphous-Si modules are produced by placing a tiny film of silicon vapor (approximately 1 µm thick) on a substrate material like glass or metal[2].

I.3.2.2 Cadmium Telluride (CdTe) Thin Film Solar Cell

Cadmium telluride (CdTe) photovoltaics is formed from cadmium telluride, a thin semiconductor layer built to design to capture and convert sunlight to electricity. Cadmium telluride PV is the sole thin film technology having less costs than traditional solar cells produced with crystalline silicon in multi-kilowatt. Basol and McCandless found that most outstanding enhancement of CdTe efficiencies occurred from 2013 to 2014 when small-area cell conversion efficiency improved to 20% range and a champion module efficiency of 17% was record [2], very recently CdTe-based solar cell has achieved 22.6%[3].

I.3.2.3 Copper Indium Gallium Di-Selenide (CIGS) Solar Cells

CIGS is a direct band gap and quaternary compound semiconductor composed of: Copper, Indium, Gallium and Selenium. The right side of **Figure 3** shows a transverse section

through a scanning electron microscope of a real device. CIGS possesses a higher efficiency than CdTe (approximately 10% - 12% on average), with some achieving an efficiency of 23.6%[3], thus competing favorably with crystalline silicon (c-Si) wafer based solar cells[2].

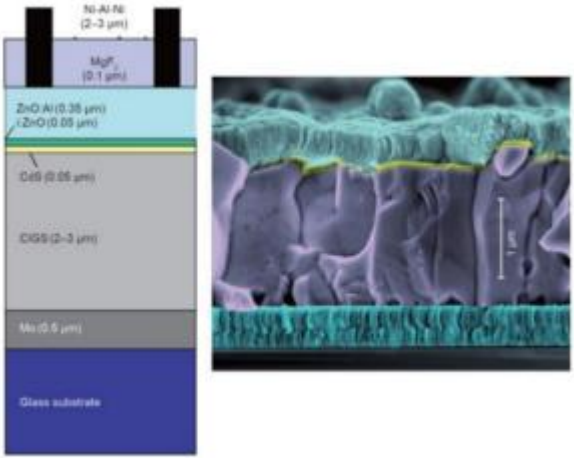


Figure 3. CIGS Solar Cell composition[2].

I.3.3 Third Generation Solar Technologies

The newly arising thin film technologies are grouped under third generation solar technologies. Most of them are not yet commercially available but under R&D phases[2].

I.3.3.1 Quantum Dot solar cells

A quantum dot (QD) is a semiconductor nanoparticle with a diameter of a few nanometers, typically 2 to 10 nm, exhibiting electrical and optical characteristics that are distinct from those of bigger particles. A quantum-dot solar cell (QDSC) is a type of solar cell in which QDs are used as the light absorbing material. By varying their size, QDs band gaps may be made programmable across a board range of energy levels, while the band gap in bulk materials is determined by the substance being used[4]. 19.1% was the highest recorded efficiency for this type of solar cell until 2023[3].

I.3.3.2 Tandem solar cells

A tandem solar cell (TSC) is a type of solar cell having different materials of different band gaps stacked together in a single structure to utilize sunlight as much as possible for the production of electrical power, as illustrated in figure 4. TSC can utilize around 86% of the solar spectrum, which is made possible by connecting cells of different band gaps. In order to utilize the solar spectrum as much as possible, different materials having different properties can be connected to form a new structure having the combined properties of the stacked materials, with an improved PCE compared to the individual materials[4].

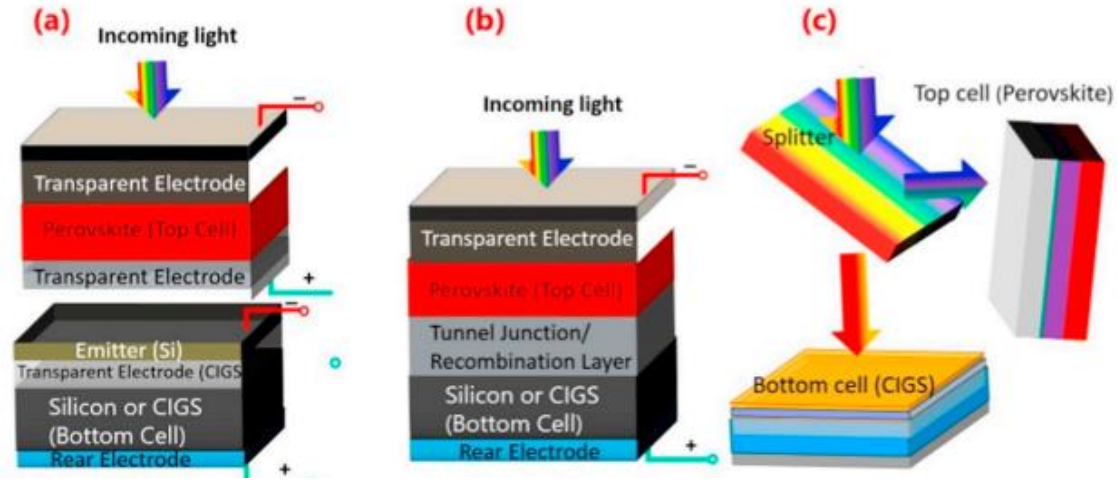


Figure 4. Shows schematic diagram of TSC, (a) mechanically stacked 4T, (b) monolithically integrated 2T, and (c) optical splitting of the solar[4].

I.3.3.3 Perovskite Solar Cells

Perovskite solar cells (PSCs) have greatly attracted the researchers, among each of the various kinds of perovskite solar cells, organic-inorganic PSCs have gotten a lot of attention because they possess the ability to be extremely affordable and produced using low-energy methods [5]. Since 2009, quick progress in hybrid PSCs has taken its place in the photovoltaic (PV) industry [6]. The efficiency of PSCs has increased significantly in a very short time, from 3.8% [6] to 26% in 2023 [7]. Recently, KAUST set the highest world record on perovskite/silicon tandem monolithic, certified with a PCE of 33.7% [3], which is incomparable with the progress in Crystalline Silicon Solar Cells (SCs) [8]. Hybrid PSCs have been attracted and considered as a promising alternative for SCs because of their interesting physical properties, such as a great absorption coefficient, a very high yield flexibility, a simple synthesis process at low temperatures (150-200 °C of thermal annealing is required at most), a high efficiency, an easy and a low cost of fabrication [9], [10], [11], [12]. These advantages come from combining the properties of inorganic and organic materials, such as a direct band gap and a high absorption coefficient in the visible range [13].

I.4 Performance characterization of solar cells

The main method for measuring the performance of a solar cell is the measurement of the density current as a function of voltage, providing J-V characteristics. In this method, a time varying bias voltage is applied to the device and at the time, the current is recorded. Typically, the time varying voltage is swept from a negative value or zero to a positive value. The output J-V characteristics can be measured while the device under test is in dark

conditions or under illumination. In the case of illumination, the device is illuminated by a light source, which is usually a solar simulator. Such a light source is designed to generate the solar radiation spectrum. Figure 5a shows a typical J-V of a solar cell in dark condition and under illumination. The dark J-V characteristic of a solar cell equals the J-V characteristic of a diode, which, for a classical p-n junction, can be described by:

$$J_D = J_0 \left(e^{\left(\frac{qv}{k\beta T}\right)}-1\right) \qquad \text{(I.1)[14]}$$

Where J, J_0, V and T are the current density, the reverse saturation current density, the applied voltage, and the temperature, respectively.

Under illumination, in steady state the photocurrent density (J_{Ph}) is created by a constant flow of photo-generated charge carriers in the opposite direction of the dark current (J_D). Therefore to obtain the current under illumination, the contribution of the photocurrent has to be subtracted from the previously described dark current (equation (1)), giving:

$$J_L = J_0 \left(e^{\left(\frac{qv}{K\beta T}\right)} - 1\right) - J_{Ph} = J_D - J_{Ph} \qquad \text{(I.2)[14]}$$

In order to calculate the power conversion efficiency (PCE) of a solar cell, the J-V characteristics under illumination are analyzed. One of the main features for evaluating the performance of a solar cell is the short circuit current density JSC (see Figure 1.4a). By definition, JSC is the current density under illumination at zero bias voltage.

$$J_{SC} = (V = 0) = -J_{Ph} \qquad \text{(I.3)[14]}$$

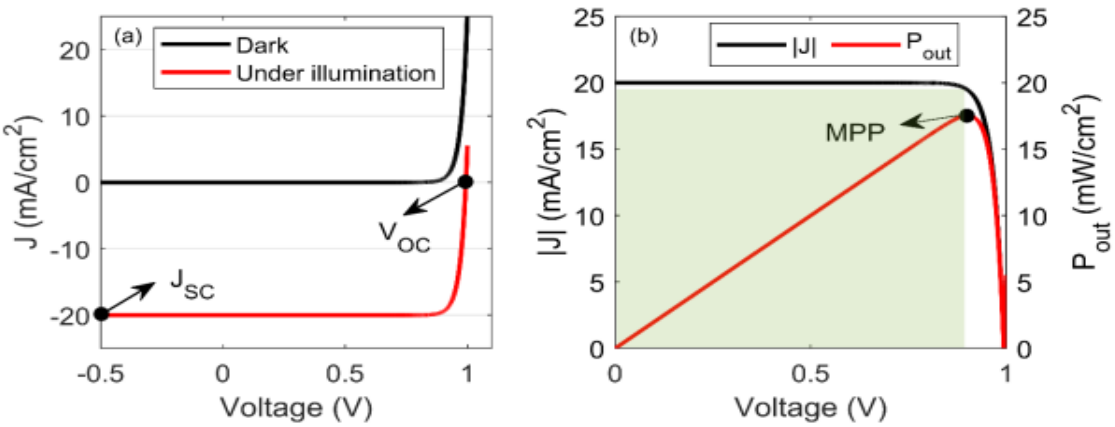


Figure 5. (a) Typical J-V characteristics of a solar cell, in dark (black line) and under illumination (red line). The corresponding V_{OC} and J_{SC} are presented in the figure. **(b)** The output power of the cell (red line) as function of voltage. The MPP of the device is presented by a black dot in the figure[14].

J_{SC} shows how many electrons and holes are generated, separated and transported toward the electrodes, and collected. The second crucial parameter for analyzing the performance of solar cells is the open-circuit voltage V_{OC} (see **Figure 1.4a**). Clearly, V_{OC} is the voltage over the device when the net current flowing through the device is zero. In fact, V = V_{OC} is the voltage at which the photocurrent exactly equals the dark current as indicated in the following equation and in the **Figure 1.4 a.**

$$J(V=V_{OC}) = J_0\left(e^{\left(\frac{qVoc}{K\beta T}\right)} - 1\right) - J_{Ph} = 0 \qquad \text{(I.4)[14]}$$

The third important parameter for evaluating the performance of solar cells is the fill factor FF. The fill factor is defined as the ratio of the maximum of the product of J and V (green shaded area in **Figure 1.4b**) and $J_{SC}\,V_{OC}$.

$$FF = \frac{\left| J_{MPP}\, V_{MPP} \right|}{J_{SC} V_{OC}} \qquad \text{(I.5)[14]}$$

Where J_{MPP} and V_{MPP} are the current density and the voltage at the maximum output power point (MPP) (see **Figure 1.4b**). In fact, the maximum output power of a solar cell is the point at where $|I \times V|$ reaches its maximum

$$P_{out} = JV \qquad \text{(I.6)[14]}$$

$$P_{out.max} = P_{out}(V_{MPP}) = \left| JV \right|_{max} = J_{SC} V_{SC} FF \qquad \text{(I.7)[14]}$$

In **Figure 1.4 b** the output power of the device is presented as a function of voltage, which shows a maximum in the range of $0<V<V_{OC}$

The PCE of a solar cells is the efficiency of the conversion of incident radiation energy into electrical energy and equals the ratio of maximum output power and the input power

$$PCE = \frac{P_{out.max}}{P_{in}} = \frac{|IV|_{max}}{P_{in} \times Area_{cell}} = \frac{|JV|_{max}}{P_{in}} = \frac{J_{SC} V_{OC} FF}{P_{in}} \quad (I.8)\ [14]$$

Here P_{in} is the input power, which is the power per unit area of the incident light on the device. $Area_{cell}$ is the active area of the device or the area that is exposed to the incident light.

Generally, the J-V characteristics and therefore the PCE of a solar cell are highly dependent on the intensity and the spectral distribution of the light as well as the temperature of the device. Thus, certain criteria for standard characterization of solar cells have been defined to facilitate the comparability of the reported results from different labs. The main conditions are a light intensity of 100 mW/cm^2 (known as 1 sun), a light spectrum with a distribution matching the globally standard solar spectrum, and a device temperature of 298 K.

For characterizing solar cells, typically white light from a solar simulator is used as the light source. Due to the mismatch between the spectrum of artificial light sources and the solar spectrum, certain modifications (such as different filters) are required to achieve a reasonable spectrum[14].

I.5 Perovskite solar cell

I.5.1 Structure of Perovskite

Perovskite means calcium titanate ($CaTiO_3$), a mineral composite first discovered in 1839, composed of calcium, magnesium and oxygen. The family of solid-state materials which poses calcium titanate structure collectivity then termed as perovskites. These two terms have been often used interchangeably. The name perovskite gave on behalf of the famous Russian mineralogist, Count Lev Alekseevich Perovski (1792-1856) and the mineral was first found out in the Ural Mountains by Gustav Rose, Victor Goldschmidt in 1926 was the first who identified the detailed perovskite crystal structure though the work on tolerance factor [15]. In a traditional view, perovskite represents a crystallographic family with the chemical formula ABX_3, in which A and B are cations and X is an anion. The ideal perovskite is a cubic structure, having B cations as six fold coordination surrounded by an octahedron of X anions, and A cations as 12 fold cub octahedral coordination, see **Figure 6** [16] [17].

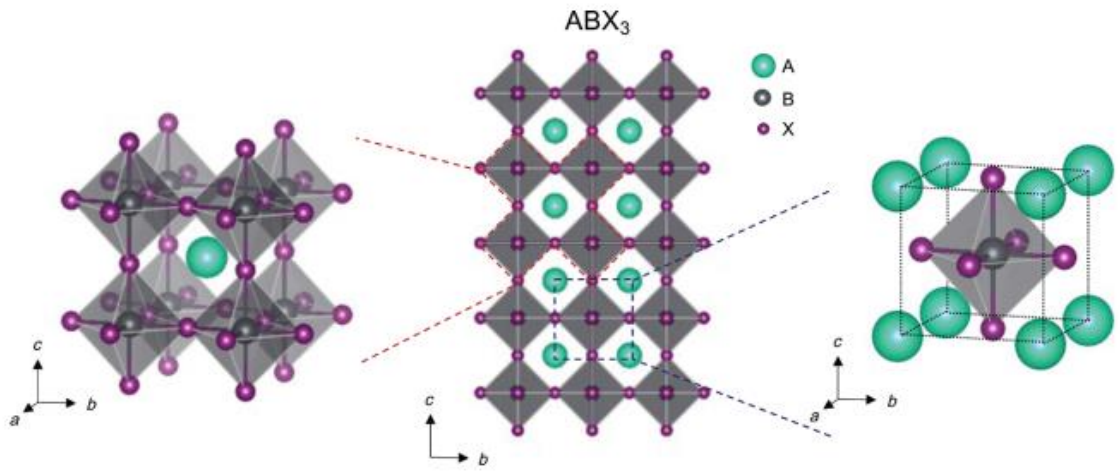


Figure 6. Crystal structure of 3D cubic perovskite. Cation A is located in the void between the BX6 octahedra. In a crystal unit cell, A is located in the corners, B is in a body-centered position, and X is in a face-centered position[18].

The highest symmetry crystal lattice for perovskite is the cubic lattice. However, the latter can be more or less distorted depending on the chemical nature of the ions that make up the perovskite. Indeed, the size of the ions (but also the distribution of their charge) plays a role in this distortion, and therefore the stability, of the crystal structure. On the basis of their atomic radii (R_A, R_B, and R_X), the Goldschmidt tolerance factor **t** makes it possible to anticipate this stability with equation (1.9):

$$t = \frac{R_A + R_X}{\sqrt{2}\,(R_B + R_X)} \quad \text{(I.9)}$$

Typically, tolerance factors of between 0.8 and 1 correspond to a cubic crystal structure whose distortion increases as it approaches 0.8. Below this value, the crystal structure generally becomes orthorhombic, and above 1, it becomes hexagonal or quadratic, thus, due to the flexibility of this crystal structure, evaluated by this tolerance factor, many chemical elements can participate in the formation of a perovskite [19]. There are therefore innumerable perovskite materials, which can be oxidized (X = oxygen) or halogenated (X = halogen) and entirely inorganic (e.g. $CaFeO_3$, $CsSnI_3$ etc.) or both inorganic and organic, so-called hybrids (e.g. $MAPbI_3$, $FAPbBr_3$ etc., MA for CH_3NH_3 and FA for $CH(NH_2)_2$). The perovskites can therefore be pure, but can also be mixed (solid solutions), where several elements and chemical species are involved (e.g. FA1-yCsyPbI3, even FA1-y-zMAzCsyPb(I1-w-xBrxClw)3 Furthermore, poor stability is attributed to the intrinsic

volatility of organic components in organic–inorganic hybrid halide perovskites such as $MAPbI_3$ ($MA = CH_3NH_3$), while the toxicity originates from lead (Pb)[20], [21]. To address such problems and find alternatives to $MAPbI_3$, extensive studies have been performed by replacing the organic component with inorganic monovalent cations like alkali cations and toxic lead with nontoxic elements such as Sn and Ge in the same group [22]. Despite extensive research on all-inorganic lead-free halide perovskites, little attention has been paid to fluoride perovskites. In this work, we propose another lead-free all-inorganic fluoride perovskite $NaSiF_3$ (A = Na, B = Si, and X=F) in order to address the physical proprieties that we need to simulate the whole solar cell using SCAPS-1D. The physical properties of $NaSiF_3$ compounds were studied using in the CASTEP code in Material studio package.

I.5.2 Structure of NaSiF3-based perovskite solar cell

The performances of photovoltaic cells based on perovskite materials depend on several parameters, such as the architecture of the cell, the materials used for the contacts, the active layer, the inter-surface layers for the transport of ETL electrons and for the transport of HTL holes as well as the techniques and the manufacturing conditions. The solar cell to be built is of the N-I-P type. The numerical simulation is carried out using the SCAPS-1D simulation software to analyze the effect of various parameters such as thickness, doping, defects and temperature on the efficiency of the perovskite solar cell structures. In our work we considered NaSiF3 as an active layer and a series of materials were used as hole transport (HTL) with electron transport material (ETL). In order to find the best combination. An efficient charge transfer, crucial for the performance of solar cells, is based on a meticulous alignment of the energy levels between the perovskite absorber and the interface layers [23]. The commonly used HTL materials must have a slightly higher occupied molecular orbital value (HOMO) compared to the absorbent layer. On the other hand, ETL materials should exhibit increased transmission in the UV region to facilitate greater penetration of photons to the absorbing layer, and the lowest unoccupied molecular orbital (LUMO) values should exceed those of the active layer [24]. Compared to the absorber, a lower conduction band (CB) level of the ETL allows electrons to flow effortlessly from the absorber to the ETL due to their natural tendency to move to lower energy states [25], [26]. Conversely, compared to the absorber, a slightly higher valence band (VB) of the HTL will effectively extract the holes when directed to the higher energy gaps in the VB of the HTL. In addition, the two electrodes should facilitate a better charge transfer from the adjacent layers and their working functions should correspond to the energy levels of the adjacent layers [27].

CHAPTER I: INTRODUCTION TO PEROVSKITE-BASED SOLAR CELLS

In this chapter, we have made state of the art on perovskite solar cell, we also presented the different structural, electronic, elastic and optical properties of $NaSiF_3$, and we have described the $NaSiF_3$-based solar cell structure.

Chapter II: simulation of Perovskite solar cell

II Simulation of Perovskite solar cell

II.1 Introduction

In this chapter, we will discuss an essential step in the new product R&D process. With the development of the computer tool, numerical simulation software and their calculation code dedicated to the field of application (finite element calculation for thermal fluidics, mechanical strength …etc.), have become the cheapest and fastest solution to replace real tests to develop new products, optimize an existing design or even opt for a technological choice over another by arguing with a simulation report. The development of photovoltaic panel cells is no exception to the rule, digital simulation tools have been created to reduce the cost of real test companions and which make it possible to make the choice of semiconductor material with the comparison criteria mentioned in the previous chapter.

II.2 BIOVIA Material Studio

BIOVIA Material Studio is a complete modeling and simulation environment designed to allow researchers in materials science and chemistry to predict and understand the relationships of a material's atomic and molecular structure with its properties and behavior. Using material studio, researchers in many industries are engineering better performing materials of all types, including catalysts, polymers, composites, metals, alloys, pharmaceuticals, batteries and more[28].

II.2.1 CASTEP

The software CASTEP (Cambridge Serial Total Energy Package) uses the theory of the functional with a defined plane wave base to crystalline solids, surfaces, molecules, liquids and amorphous materials of first principles of density. It was created in the 1980s and early 1990s in the TCM group of the Cavendish Laboratory in Cambridge[29]. This is then a code academic written in Fortran77. In the mid-1990s, it was marketed by international license in Molecular Simulations (the company was bought by Accelrys, at its tower purchased by BIOVIA) in an arrangement by which share of the royalties, and there is still a lot left of the find-tuning with the authors original academics. The code was rewritten then around 2001 to make use of features of modern Fortran[30].

Based on the pseudo potential method to provide a level with a good description of all kinds of materials and molecules. CASTEP is used to calculate the total energies, forces and constrains of an atomic system, as well as the calculation of the optimal geometry, the band

structures, optical spectra, phonon spectra and much more, it can also perform molecular dynamics simulation[30].

The CASTEP code requires the introduction of the space group, mesh parameter and choice of the pseudo-potentials of the material to be simulated and the type of the functional (LDA. GGA. etc…), and the choice of ultrafine calculation takes into account the parameters of optimal convergences[30].

II.2.1.1 Calculation method

CASTEP uses a free file format so that only specific commands required for a given calculation must be given. The values of all the variables input have default settings, with intelligent selection of parameters essential such as the base size (plane wave cut-off energy), the sets of points k, Fourier transform networks, etc. The command line running the code is simple with an output file summarizing the calculation as it proceeds and a binary format file containing the details such as the wave function coefficients and the load densities. In addition, there is a command-line help function[30].

A graphical user interface is available at Accelrys, Inc., namely the package Material Studio which can be used to build the initial structure, generate files input, execute the calculation and finally analyze the data. It can be easily used to create charge density isosurfaces, to visualize the band structures, to analyze phonon data and so on[30].

II.2.1.2 Functionality

The physical properties of materials that can be calculated using CASTEP includes[31]:

- **Total energy :**

Calculation of the total energy of forces, stresses and elastic constants.

- **The electronic structure :**

Density of electronic charges, orbital, potentials, electrostatic, structure of bands, the electron density of the total and partial states, the population analysis of Mulliken and optical properties (such as reflectivity, absorption refractive index, the dielectric function).

- **The geometry:**

Optimization of the atomic positions and the parameters of the unit cell either constrained or unconstrained.

- **Molecular dynamics:**

The molecular dynamics of the finite temperature can be realized under various conditions such as constant temperature, energy, volume and pressure.

- **Transitional state:**

The LST/QST methods are used to find the transition states.

- **The Phonons:**

We calculate the density functional perturbation theory (DFPT), eigenvectors and the frequencies of the phonons which can be used to give the free energy of Gibbs, the entropy, the enthalpy, the debye temperature, the heat capacity and a measurement of phase stability.

- **The electric field response:**

The response of the system of an external electric field which gives polarizabilities in volume, dielectric constants, effective charge terminal, LO/TO for separation of the phonons and the IR intensity of the phonon modes.

- **Exchange and correlation:**

The well-known functions of LDA and GGA are included (by the functions PW91, EPB, RPBE) but non-local functions such as the weighted density approximation (EDW), Hartree Fock and exact/exact exchange are also available.

II.3 Presentation of SCAPS-1D

SCAPS-1D acronym for “Solar Cell Capacitance Simulator one dimension” is a program developed at the University of Ghent in Belgium with Windows/CVI National Instruments by Marc Burgelman et al. this program is designed specifically for the simulation of photonic devices such as CdTe and CIGS cells. This software has several advantages, among the main advantages of SCAPS-1D:

The high speed of exaction

- The ease of exporting the results obtained (the results obtained are in text format)
- The possibility of introducing seven semiconductor layers
- The possibility of introducing interfaces and taking into account the phenomenon of recombination and the levels of defects therein.

SCAPS-1D explores the fundamental properties such as:

- ✓ The open-circuit voltage V_{OC},
- ✓ The current density J_{SC},
- ✓ The characteristics of I-V voltage,
- ✓ The capacitance-frequency (C-f),
- ✓ The efficiency of the power conversion of the device η,
- ✓ Quantum efficiency QE,
- ✓ The filling factor FF.

In the SCAPS-1D start panel (see **Figure 7)**, there are several sections, numbered from 1 to 6.

Section 1 shows that the problem box makes it possible to define a complete solar cell structure containing several layers and physical properties. In section 2, the action box makes it possible to define the parameters of the I-V characteristics scale, the parameters of the quantum efficiency measurement scale (QE or IPCE), the scale (C-V) as well as the capacitance-frequency (C-f). In section 3, the illumination box allow you to select the light and dark conditions for the simulation and the required spectrum file. In section 4, the box of the working point makes it possible to define the working temperature and to describe the parasitic resistors, such as series and branch resistors. Section 5 allows you to perform single calculations, batch calculations and curve fitting calculations. Recording and script configuration options are also available. Finally, in section 6, the "calculation results" box gives the options to check the results of the simulated device, such as the energy band (EB), I-V, QE characteristics, etc.

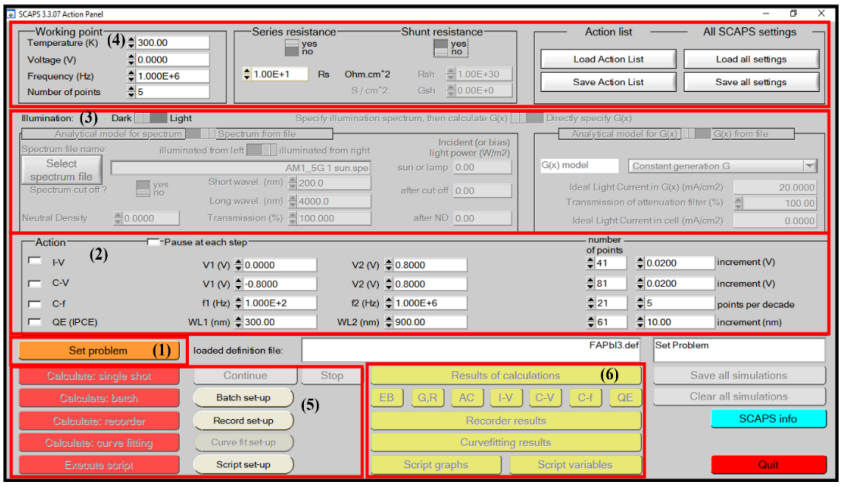


Figure 7. SCAPS-1D software startup control panel[32].

Starting the construction of the solar cell structure by clicking on section one, **Figure 8** shows the three different sections that are available and offer the options to build the desired solar cell structure with/without the interface layer.

Section 1 helps us define the different layers to complete the structure of the device, including the front and rear contact. Section 3 presents the constructed device, and there are other options for selecting the light illumination and the sides of the applied voltage using either the front contact side or the rear contact side. Section 3 allows you to create a new structure file or to load the available file and save the structure file of the required device.

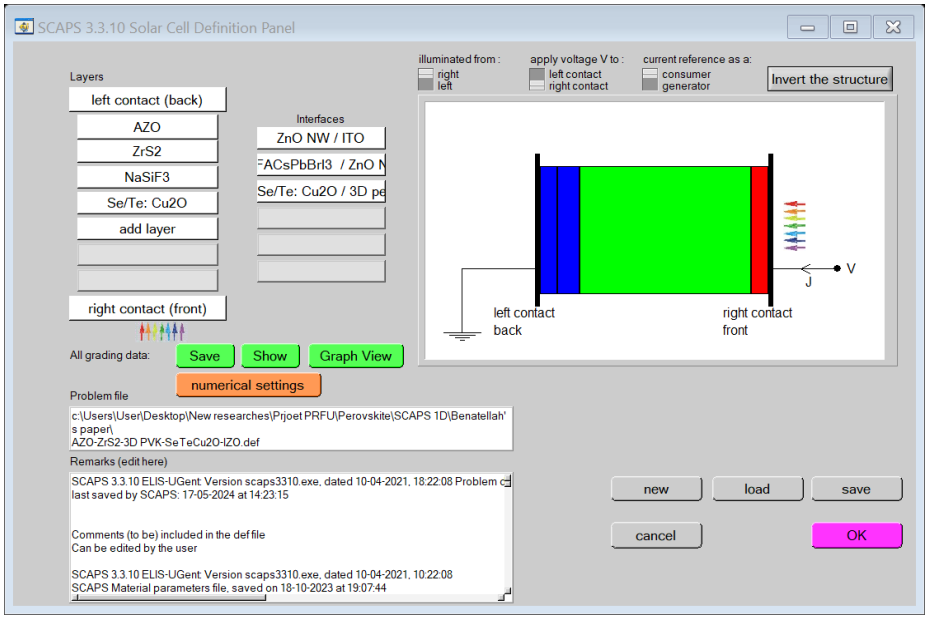


Figure 8. SCAPS-1D solar cell definition panel with perovskite structure.

Figure 9 presents the panel of defining the materials and the defects, which makes it possible to define the physical parameters of each layer, such as E_g (gap energy), □ (electron affinity), ε (dielectric constant), N_C (density of states of the conduction band), N_V (density of states of the valence band), μ_N (mobility of the electrons), μ_P (the mobility of the holes), N_A (concentration of the acceptor dopant), N_D (concentration of the donor dopant)…etc.

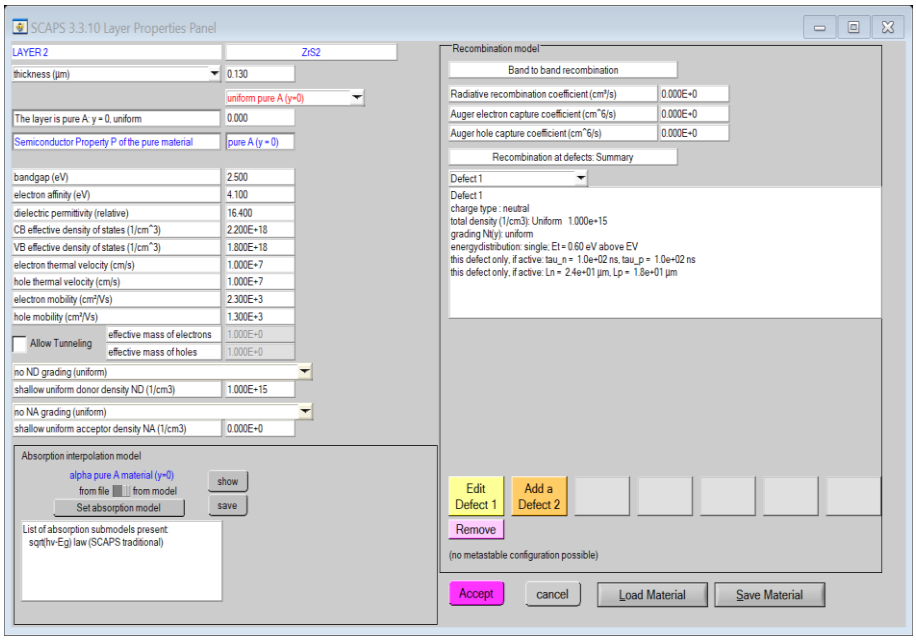


Figure 9. Panel for defining the physical properties of the layers.

II.3.1 Solar cell structure

The performances of photovoltaic cells based on perovskite materials depend on several parameters, such as the architecture of the cell, the materials used for the contacts, the active layer, the interfacial layers for the transport of ETL electrons and for the transport of HTL holes as well as the techniques and the manufacturing conditions[33].

In our work we considered $NaSiF_3$ as the active layer and Se/Te as a hole transport material (HTL) with ZrS_2 as electron transport material (ETL).

The solar cell to be built is of the P-I-N type. The numerical simulation is carried out using the SCAPS-1D simulation software to analyze the effect of various parameters such as thickness, doping, defects and temperature on the efficiency of the perovskite solar cell structure.

Table II-1 shows the parameters of the layers that build the perovskite solar cells, we will use these parameters to simulate the short-circuit current, the open circuit voltage, Fill Factor and cell efficiency in this cell.

Table II-1:Parameters used for the simulation of the structure of solar cells in perovskite[34].

Parameters	**AZO**	**ZrS_2**	**$NaSiF_3$**	**Se/Te:Cu_2O**
Thickness (nm)	100	100	3000	100
Bandgap (eV)	3.10	2.5	1.17	1.88
Electron affinity (eV)	4.1	4.1	3.9	3.53
Dielectric permittivity (relative)	9.00	16.4	24.1	7.11
CB effective density of states ($1/cm^3$)	1.1×10^{17}	2.2×10^{18}	1×10^{17}	2.02×10^{17}
VB effective density of states ($1/cm^3$)	1.0×10^{18}	1.8×10^{19}	1×10^{17}	1.17×10^{19}
Electron thermal velocity (cm/s)	1.0×10^{7}	1.0×10^{7}	1.0×10^{7}	1.0×10^{7}
Hole thermal velocity (cm/s)	1.0×10^{7}	1.0×10^{7}	1.0×10^{7}	1.0×10^{7}
Electron mobility (cm^2/Vs)	100	2.3×10^{3}	2.2	1297
Hole mobility (cm^2/Vs)	25	1.3×10^{3}	2.2	1297
Shallow uniform acceptor density N_A ($1/cm^3$)	0	1×10^{15}	1×10^{14}	3.0×10^{18}
Shallow uniform donor density N_D ($1/cm^3$)	1.0×10^{15}	0	1×10^{14}	0
Defect type				
N_t total ($1/cm^3$) uniform	1.0×10^{10}	1×10^{15}	/	1.0×10^{15}
Reference	[35]	[36]	This study	[37]

Chapter III: Results and discussions

III Results and discussions

III.1 DFT simulation

Our calculation were carried out using the CASTEP code. It is code based on the theory of the density functional. The wave functions are developed on a wave basis planes in association with pseudo-potential technique. The pseudo-potential to norm it has been used with the configurations: $1s^2\ 2s^2\ 2p^6\ 3s^1$ for Sodium (Na), $1s^2\ 2s^2\ 2p^6\ 3s^2\ 3p^2$ for Silicon (Si), and $1s^2\ 2s^2\ 2p^5$ for Fluor (F). We have used the following parameters: space group n° **221**, a=b=c=4.28 Å and α=β=γ=90°, Energy cut-off of 400 eV, 12×12×12 K-point, Energy 10^{-5} Ev/atom, Max force 0.03 Ev/Å, Max stress 0.05 GPa, and displacement 0.001 Å.

III.2 Crystalline structure

Figure 10 represent the cubic structure of the $NaSiF_3$ cell with the parameters of the following experimental methods: a=b=c=4.28Å and α=β=γ=90°.

The structure of the simulation shows that the cubic structure contains one Sodium atom, one Silicon atom and three Fluor atoms with the following positions:

$Na(0 \quad 0 \quad 0)$

$Si\left(\frac{1}{2} \quad \frac{1}{2} \quad \frac{1}{2}\right)$ $\qquad$ $F\left(0 \quad \frac{1}{2} \quad \frac{1}{2}\right)$

$F\left(\frac{1}{2} \quad 0 \quad \frac{1}{2}\right)$ $\qquad$ $F\left(0 \quad \frac{1}{2} \quad \frac{1}{2}\right)$

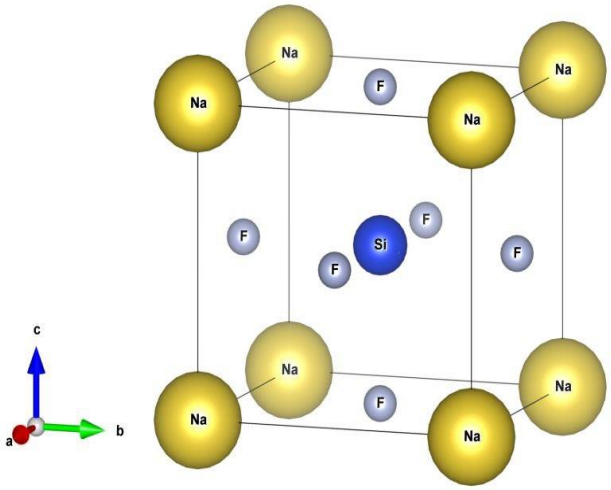


Figure 10. Crystalline structure of $NaSiF_3$.

The phase diversity of ABX_3 systems can be qualitatively described using the tolerance factor t giving by equation:

$$t = (r_A + r_X)/\sqrt{2}(r_B + r_X) \qquad \text{(III.1)}$$

In our study, we have $NaSiF_3$ perovskite structure. We can calculate the tolerance factor as follows:

$$t = (r_{Na} + r_F)/\sqrt{2}(r_{Si} + r_F) \qquad \text{(III.2)}$$

With: $r_{Na} = 1.02$ Å

$r_{Si} = 0.26$ Å

$r_F = 1.33$ Å

A perovskite cubic structure stability occurs if 0.84<t<1.10[38]. When we calculate the tolerance factor of $NaSiF_3$ perovskite structure we find it equal 1.04 (other work t=0.96[39]), and this result means that this cell is stable.

III.3 Band structure

We have studied the band structure of $NaSiF_3$ perovskite material. **Figure 11** shows that the conduction band (CB) minimum is located at the R point and the valence band (VB) are maximum is located at the Γ point. This result indicates that $NaSiF_3$ semiconductors have indirect band gap (Eg= 0.618 Ev).

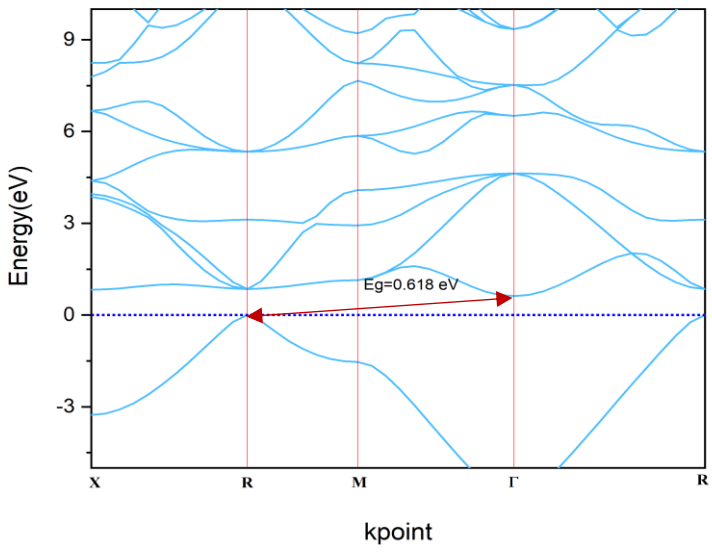


Figure 11. Electronic band structure of $NaSiF_3$.

III.4 Total and partial density of state

The probability of electron dispersion in the energy spectrum is defined by the density of state (DOS). The examination of the total and partial density of state (TDOS and PDOS) diagram in **Figure 12**, can be used to determine the origin of states that made up the valence band and conduction band of the $NaSiF_3$ perovskite material[39].

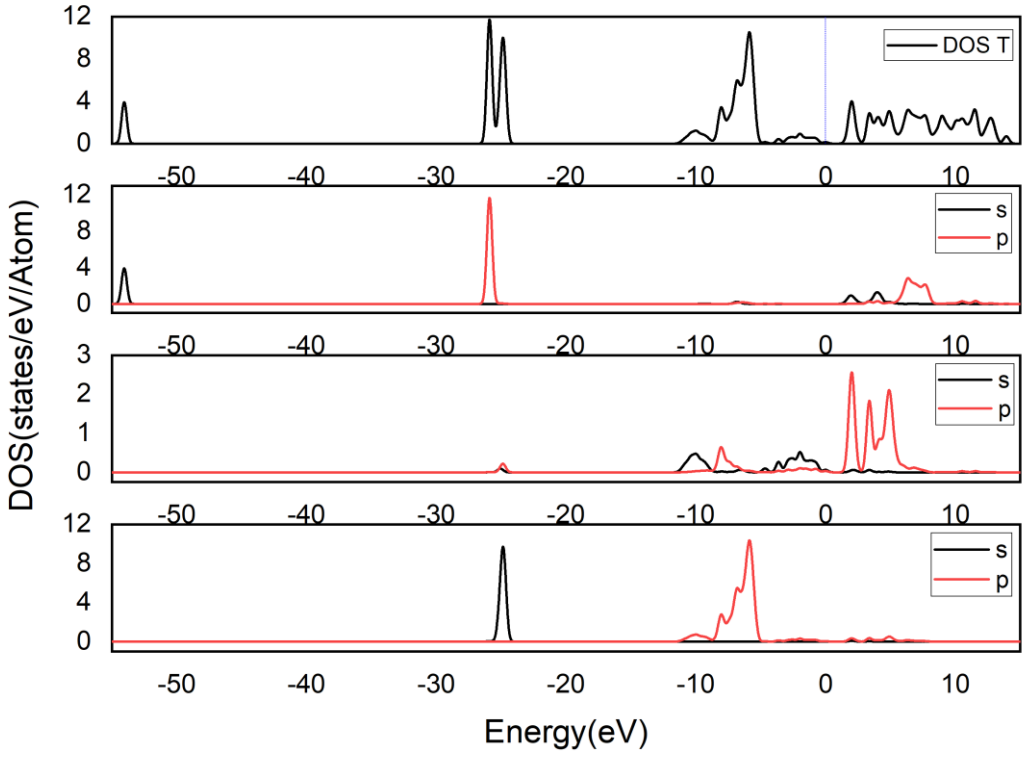


Figure 12. Total and partial DOS of $NaSiF_3$.

- The included valence band region is at 54 eV and originates from one of highly participating orbitals Na(s).
- The two peaks produced in the region [-26eV and -25eV] and [-25eV and -24eV], come from the participation of the orbitals Na(p) and F(s),respectively.
- The orbital F(p) make up the majority of participation in the four peaks produced in the region [-11eV and -5eV] and a tiny participation of Si(s) and Si(p).
- The peaks produced in the region [-5eV and 0eV], come from the participation of the orbital Si(s).

- In the conduction band, we have 4 peaks in the region [1eV and 8eV], come from a tiny participation of Na(s) and majority of Si(p) in the region [1eV and 5eV], and high participation of Na(p) in the region [5eV and 8eV].

III.5 Elastic properties

Single-crystal elastic constants C_{ij} deliver information concerning the strength of a solid, describe its resistance against external forces and help avoid material failure in engineering design. The cubic lattice balance is such that the 21 dependent elastic constants are reduced to three independent elastic constants (C_{11}, C_{12} and C_{44}). The C_{11} constant is related to the unidirectional compression along the principal crystallographic directions, whereas constants C_{44} and C_{12} are involved in shear deformation resistance[39]. **Table III-1** represent values of calculated elastic constants C_{ij} of $NaSiF_3$ perovskite material.

Table III-1: Values of calculated elastic constants C_{ij}.

$NaSiF_3$	C_{11}	C_{12}	C_{44}
Our work	84.93	38.01	6.70
Other work	85.97[39]	38.43[39]	6.62[39]

We are considered a cubic crystal structure, mechanically stable when the elastic constants satisfy the following criteria of stability [39]:

$$(C_{11} - C_{12}) > 0; (C_{11} + 2C_{12}) > 0; C_{44} > 0 \quad [39]$$

When we compare our calculated elastic constants with the criteria of stability, we find that these criteria are satisfied. This indicates that $NaSiF_3$ compound has elastic stability.

III.6 Optical properties

The electrical and optical properties of the material are affected when it interacts with electromagnetic waves, and this is determined by the complex dielectric function ε(x) that describes its optical properties. This function can be written as[38]:

$$\varepsilon(\omega) = \varepsilon_1(\omega) + i\varepsilon_2(\omega) \qquad \text{(III.3)}$$

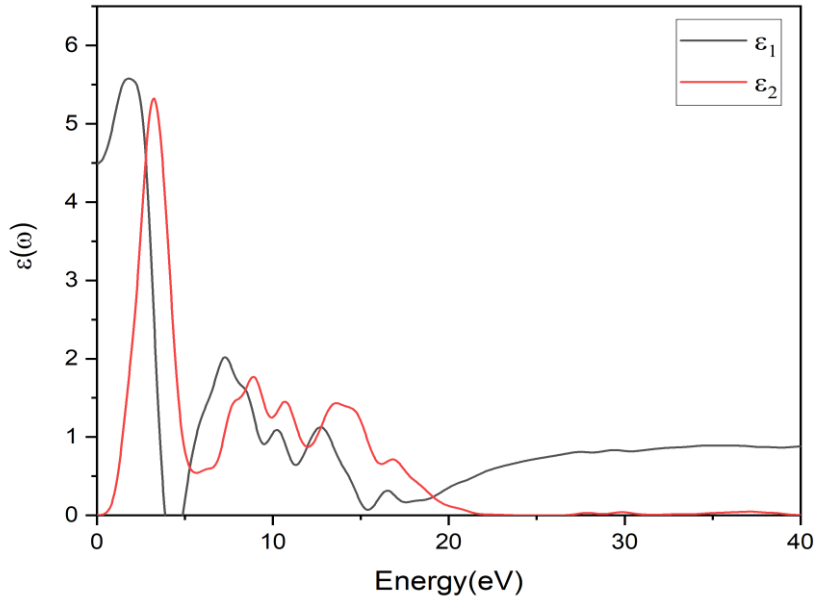


Figure 13. Computed dielectric imaginary part ε2(ω) and dielectric real part ε1(ω) for the NaSiF3.

The complex dielectric function (ε) is divided into two parts. Firstly, (ε_1) corresponds to polarization; secondly, (ε_2) expounds on the energy dissipation in the system.

$$\varepsilon_1(\omega) = 1 + \frac{2}{\pi} P \int_0^{\infty} \frac{\omega' \varepsilon_2(\omega')}{\omega'^2 - \omega^2} d\omega' \qquad \text{(III.4)}$$

Where P is the principal value of the integral

$$\varepsilon_2(\omega) = \frac{2e^2\pi}{\Omega\varepsilon_0} \sum_{k,\upsilon,c} |\psi_k^c| u.r |\psi_k^{\upsilon}|^2 \delta(E_k^c - E_k^{\upsilon} - E) \qquad \text{(III.5)}$$

Where subscripts k,υ,c represent the reciprocal lattice vector, the conduction band, and the lower valence band, u,ω,e,ψ_k^c,and ψ_k^{υ} are the incident electric field polarization vector, light frequency, electronic charge, and conduction and valence band wave functions at k, respectively, and E_k^c, and E_k^{υ} are intrinsic energy levels[38].

Figure 13 shows the computed dielectric functions of $NaSiF_3$. Peak at 4.49 eV suggests that $NaSiF_3$ has strong dielectric properties and significant light absorption near the Ultraviolet (UV) region. The response in both ε_1 and ε_2 diminishes significantly beyond 20eV indicate that $NaSiF_3$ have a minimal absorption at higher energies.

Optical coefficients, including the refractive index n(ω), extinction coefficient k(ω), absorption coefficient α(ω), reflectivity R(ω), and energy loss coefficient L(ω) can be determined from the dielectric function using the following relations[38]:

$$n(\omega) = \left(\sqrt{\varepsilon_1^2(\omega) + \varepsilon_2^2(\omega)} + \varepsilon_1(\omega)\right)^{\frac{1}{2}} \Big/ \sqrt{2} \qquad \text{(III.6)}$$

$$k(\omega) = \left(\sqrt{\varepsilon_1^2(\omega) + \varepsilon_2^2(\omega)} - \varepsilon_1(\omega)\right)^{\frac{1}{2}} \Big/ \sqrt{2} \qquad \text{(III.7)}$$

$$\alpha(\omega) = \sqrt{2\omega}\left(\sqrt{\varepsilon_1^2(\omega) + \varepsilon_2^2(\omega)} - \varepsilon_1(\omega)\right)^{\frac{1}{2}} \qquad \text{(III.8)}$$

$$R(\omega) = \left| \frac{\varepsilon(\omega)^{\frac{1}{2}} - 1}{\varepsilon(\omega)^{\frac{1}{2}} + 1} \right|^{\frac{1}{2}} \qquad \text{(III.9)}$$

$$L(\omega) = \frac{\varepsilon_2(\omega)}{\varepsilon_1^2(\omega) + \varepsilon_2^2(\omega)} \qquad \text{(III.10)}$$

The refractive index is a fundamental optical property that influences how light propagates through a material. It is the ratio between the speed of light in vacuum and the speed of the light in the material. **Figure 14** shows the computed refractive index η(ω) of $NaSiF_3$. The graph indicate that $NaSiF_3$ has a strong refractive properties at 2.41 at low energy (2.38eV), and minimal interaction at high energies.

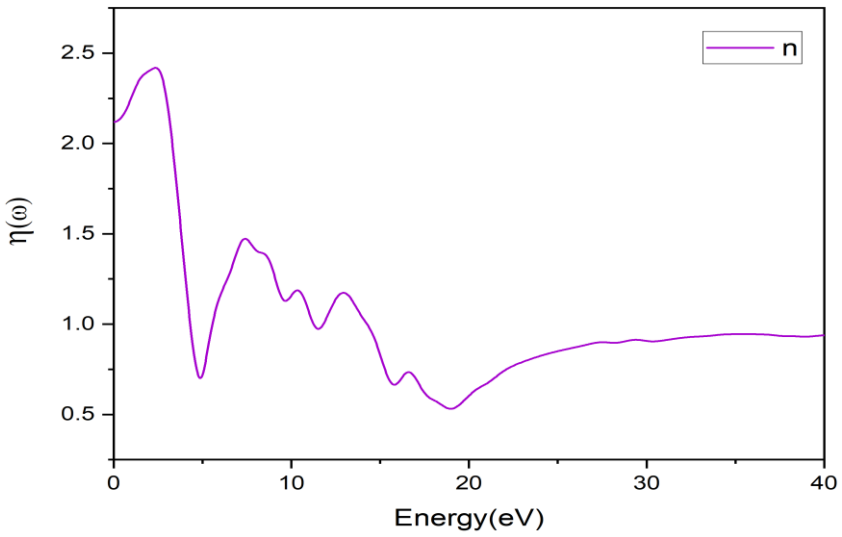


Figure 14. Computed refractive index η (ω).

In the context of optics and materials sciences, the extinction coefficient is important for understanding how a material interacts with electromagnetic radiation, particularly in applications involving light absorption, reflection, and transmission. **Figure 15** shows the extinction coefficient K(ω) of $NaSiF_3$). The extinction coefficient rapidly increases in region [0eV – 1eV] and then deceases. The peak in this region indicate a strong absorption of light of $NaSiF_3$. In high energies [20eV-40eV], the extinction coefficient becomes very small, and this implies that there are no significant absorption.

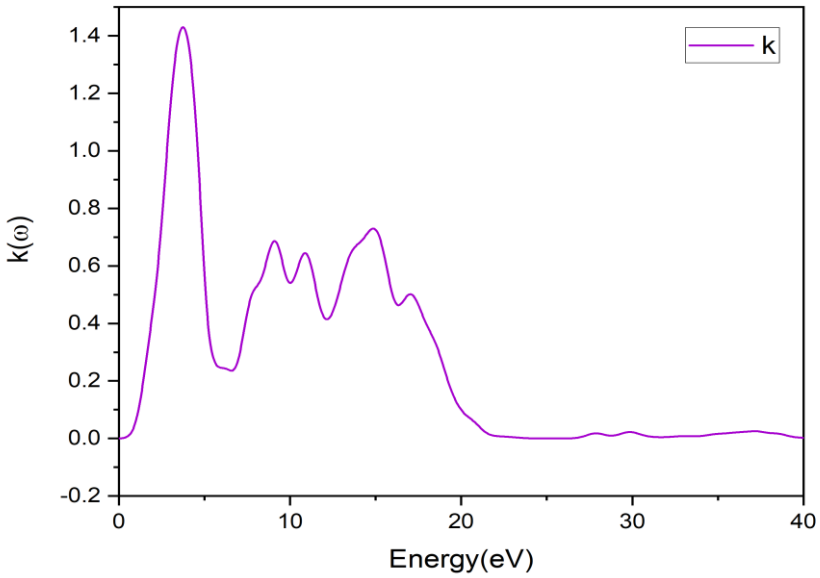


Figure 15. Computed extinction coefficient k (ω).

The absorption coefficient indicates how much light of a specific energy is absorbed per centimeter of the material. **Figure 16** shows the absorption coefficient of $NaSiF_3$ as a function of energy. The highest absorption occurs in 15 eV with the peak value at 1.8×10^{-5} cm^{-1}. After 20 eV, the absorption coefficient drops, this indicate that $NaSiF_3$ absorbs less light in high energies. This behavior means that $NaSiF_3$ can be used in optoelectronic applications, where the absorption spectrum is important for determining the efficiency of light absorption and conversion into electric energy.

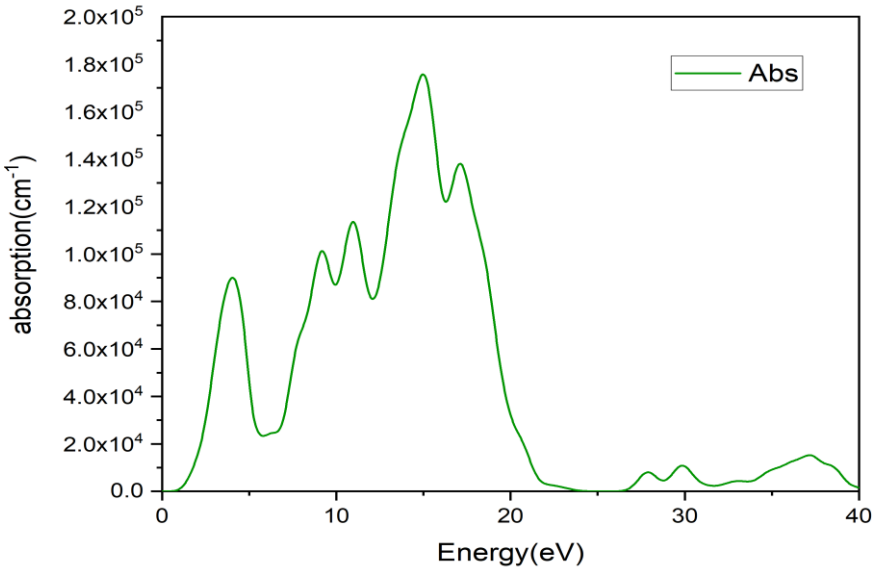


Figure 16. Absorption coefficient for NaSiF3.

Reflectivity is a measure of how much light is reflected by a material's surface and is important for understanding the optical properties of materials. **Figure 17** shows the reflectivity R(ω) of $NaSiF_3$. There are several peaks in the reflectivity spectrum, the highest reflectivity is observed in 4 eV with 0.28 (28% reflectivity), and after 25 eV the reflectivity is low, this indicate that $NaSiF_3$ reflect less light at higher energies.

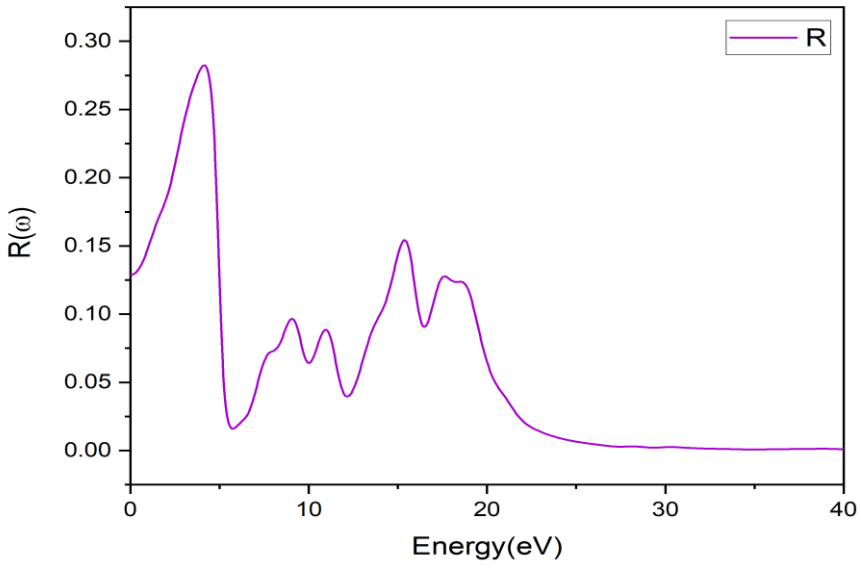


Figure 17. Reflectivity of NaSiF3 R (ω).

The energy-loss function provides insight into how energy is lost by electrons as they pass through the material. **Figure 18** represents the energy-loss spectrum L(ω). The highest peak occurs at 18 eV with a value of energy-loss 2.25 indicate a significant energy loss.

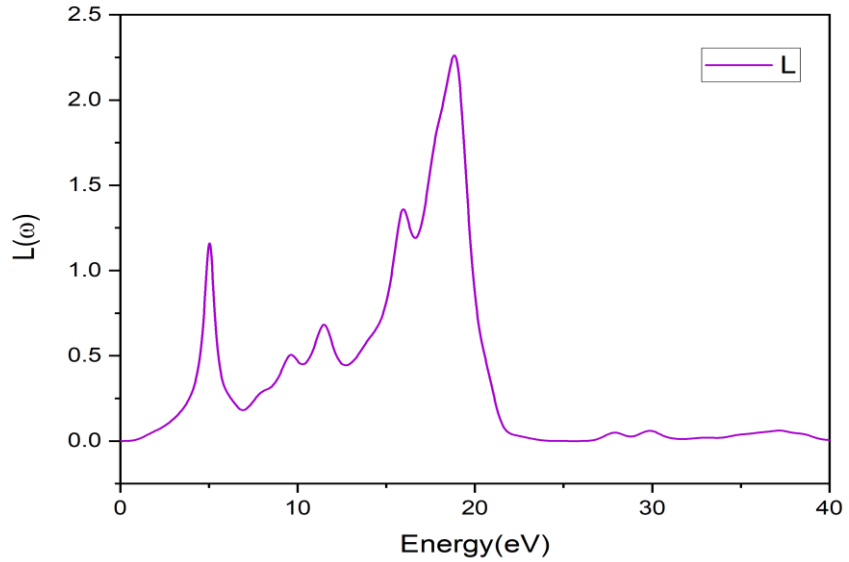


Figure 18. Energy-loss spectrum L (ω).

III.2 SCAPS-1D simulation:

Based on the results of the DFT, we have extracted some inputs that we will need to launch a simulation of the electrical behavior of a solar cell with a p-i-n structure Se:Te/CuO_2/$NaSiF_3$/ZrS_2/AZO. Figure shows the characteristic J-V of a perovskite solar cell. The photovoltaic parameters of this cell shows in the following table:

Table III-2: Photovoltaic parameters of Te/CuO_2/$NaSiF_3$/ZrS_2/AZO perovskite solar cell.

Parameters	V_{OC} (V)	J_{SC} (mA/cm^2)	FF (%)	PCE (%)
Cell structure	0.749439	3.91	77.79	2.28

These parameters have a very low performance and they are very low compared with perovskite solar cells, where the latter retain very high efficiencies reaching up to 26.1%. To improve the performance of this cell, it is necessary to improve the properties of the $NaSiF_3$ active layer and it will be like a perovskite for the next work on this new materials.

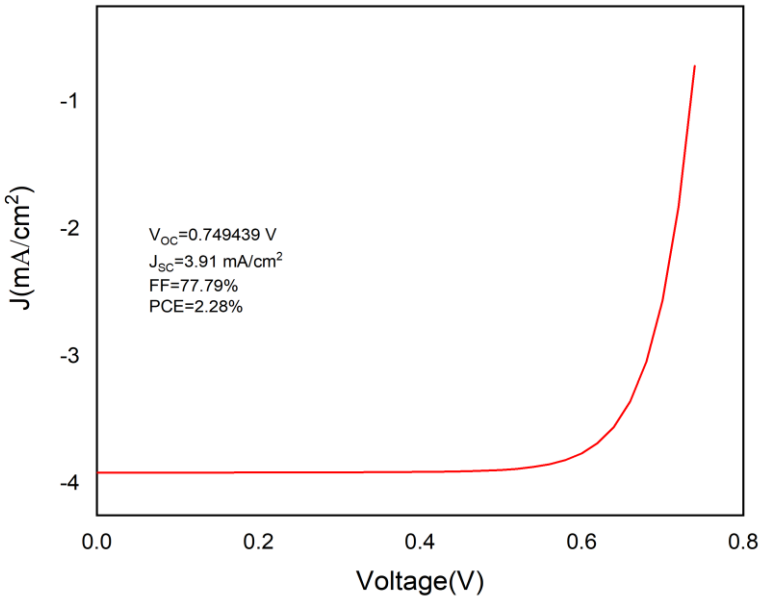


Figure 19. J-V curve of Se:Te/CuO_2/ $NaSiF_3$/ ZrS_2/ AZO.

General Conclusion

Perovskite has been the subject of research over the past two decades, solar cells based on perovskite-based structured materials have attracted great attention over the past year, especially inorganic materials such as $NaSiF_3$.

Therefore, we first conducted a brief state of the art of solar cells, the photovoltaic technologies, the performance characterization of solar cells, and the perovskite solar cells. Then we moved on to talk about our material $NaSiF_3$.

Our project was a mixture of a theoretical study of the properties of $NaSiF_3$ perovskite and a numerical modulation based on the parameters extracted from the DFT of the active layer. We studied the structural, electronic, elastic, mechanical and optical properties of $NaSiF_3$. According to the DFT we found that the $NaSiF_3$ material has an inert gap of the order of 0.6831 eV and an absorption coefficient of the order of 2×104 cm^{-1}. A modilization of the solar cell based on perovskite, using the SCAPS software has been done. The model of the cell with the structure P-I-N Se/Te/CuO_2/$NaSiF_3$/AZO/ZrS_2 was created and simulated as the first linker. The results of the simulation show that the performance of the cell was significantly low. We concluded that the efficiency of the cell reaches its minimum value, al because of their electrical properties will take place in the future works in order to obtain high yields.

References

[1] L. L. Kazmerski, “Solar photovoltaics R & D at the tipping point : A 2005 technology overview,” vol. 150, pp. 105–135, 2006, doi: 10.1016/j.elspec.2005.09.004.

[2] K. E. Sarah, P. U. Roland, and P. O. E. N. C, “A Review of Solar Photovoltaic Technologies,” no. January, 2024.

[3] NREL, “Best Research-Cell Efficiency Chart | Photovoltaic Research | NREL.”

[4] N. Shah *et al.*, “A Review of Third Generation Solar Cells,” 2023.

[5] M. Hauck, T. Ligthart, M. Schaap, E. Boukris, and D. Brouwer, “Environmental benefits of reduced electricity use exceed impacts from lead use for perovskite based tandem solar cell,” *Renew. Energy*, vol. 111, pp. 906–913, 2017, doi: 10.1016/j.renene.2017.04.044.

[6] A. Kojima, K. Teshima, Y. Shirai, and T. Miyasaka, “Organometal Halide Perovskites as Visible-Light Sensitizers for Photovoltaic Cells,” *J. Am. Chem. Soc.*, vol. 131, no. 17, pp. 6050–6051, 2009, doi: 10.1021/ja809598r.

[7] Y. Zhao *et al.*, “Supplementry Materials: Inactive (PbI2)2RbCl stabilizes perovskite films for efficient solar cells,” *Science (80-.).*, vol. 377, no. 6605, pp. 531–534, 2022, doi: 10.1126/science.abp8873.

[8] Lin H *et al.*, “26.7% Efficiency Silicon Heterojunction Solar Cells Achieved By Electrically Optimized Nanocrystalline-Silicon Hole Contact Layers,” *Nat. Energy*, vol. 8, pp. 789–799, 2023, doi: 10.1038/s41560-023-01255-2.

[9] P. Fooladvand, M. Eskandari, D. Fathi, and N. Das, “Single-walled carbon nanotube as hole transport layer in perovskite solar cell: Efficiency enhancement,” *Energy Reports*, vol. 10, no. October, pp. 3652–3664, 2023, doi: 10.1016/j.egyr.2023.10.020.

[10] N. R. Pochont and Y. R. Sekhar, “Numerical Simulation of Nitrogen-Doped Titanium Dioxide as an Inorganic Hole Transport Layer in Mixed Halide Perovskite Structures Using SCAPS 1-D,” *Inorganics*, vol. 11, no. 1, pp. 1–17, 2023, doi: 10.3390/inorganics11010003.

[11] C. Li *et al.*, “An ultrahigh 84.3% fill factor for efficient CH3NH3PbI3 P-i-N perovskite film solar cell,” *Sol. Energy*, vol. 233, no. February, pp. 271–277, 2022, doi: 10.1016/j.solener.2022.01.035.

[12] S. Sansoni *et al.*, “Eco-Friendly Spray Deposition of Perovskite Films on Macroscale Textured Surfaces,” *Adv. Mater. Technol.*, vol. 5, no. 2, pp. 1–6, 2020, doi: 10.1002/admt.201901009.

[13] Y. Raoui, H. Ez-Zahraouy, N. Tahiri, O. El Bounagui, S. Ahmad, and S. Kazim, “Performance analysis of MAPbI3 based perovskite solar cells employing diverse charge selective contacts: Simulation study,” *Sol. Energy*, vol. 193, no. October, pp. 948–955, 2019, doi: 10.1016/j.solener.2019.10.009.

[14] M. S. Alvar, “D EVICE P HYSICS O F P EROVSKITE S OLAR C ELLS,” no. September, 2020.

[15] S. C. Mouna *et al.*, “Physical properties of Be-based fluoroperovskite compounds XBeF3 (X = K, Rb): a first-principles study,” *J. Phys. Condens. Matter*, vol. 36, no. 5, 2024, doi: 10.1088/1361-648X/ad05f9.

[16] T. Lemercier, “Développement de cellules solaires pérovskites semi-transparentes de type P-I-N dans la perspective d’une application tandem,” UNIVERSITÉ SAVOIE MONT BLANC, 2020.

[17] H. Narayanan, “Perovskite materials-an introduction,” no. April, 2023.

[18] T. Duan and Y. Zhou, “Introduction to Perovskite 1 . 1 Evolution of Perovskite,” pp. 1–8, 2024.

[19] Z. Li, M. Yang, J. S. Park, S. H. Wei, J. J. Berry, and K. Zhu, “Stabilizing Perovskite Structures by Tuning Tolerance Factor: Formation of Formamidinium and Cesium Lead Iodide Solid-State Alloys,” *Chem. Mater.*, vol. 28, no. 1, pp. 284–292, 2016, doi: 10.1021/acs.chemmater.5b04107.

[20] H. Alipour and A. Ghadimi, “Optimization of lead-free perovskite solar cells in normal-structure with WO3 and water-free PEDOT: PSS composite for hole transport layer by SCAPS-1D simulation,” *Opt. Mater. (Amst).*, vol. 120, no. July, pp. 1–8, 2021, doi: 10.1016/j.optmat.2021.111432.

[21] C. V. Rudrappa and S. Ganesan, “Investigation of performance and stability of multilayered organometallic halide Perovskite cell,” *J. Integr. Sci. Technol.*, vol. 11, no. 1, p. 465, 2022.

[22] C.-J. Pak, U.-G. Jong, C.-J. Kang, Y.-S. Kim, and Y.-H. K. and C.-J. Yu, “First-

principles study on the optoelectronic and mechanical properties of all-inorganic lead-free fluoride perovskites ABF3 (A = Na, K and B = Si, Ge)," *Mater. Adv.*, vol. 4, no. 4528, pp. 4528–4536, 2023, doi: 10.1039/d3ma00457k.

[23] P. Schulz, D. Cahen, and A. Kahn, "Halide Perovskites: Is It All about the Interfaces?," *Chem. Rev.*, vol. 119, no. 5, pp. 3349–3417, 2019, doi: 10.1021/acs.chemrev.8b00558.

[24] S. Karthick, "Formamidinium- Cesium (FA-Cs) based hybrid perovskite solar cells: A comprehensive simulation and experimental analysis.," CENTER FOR RESEARCH AND ADVANCED STUDIES OF THE NATIONAL POLYTECHNIC INSTITUTE, 2021.

[25] M. D. Shahjahan *et al.*, "Halide Perovskite Single Crystals and Nanocrystal Films as Electron Supplementary Information for Halide Perovskite Single Crystals and Nanocrystal Films as," *Angew. Chemie Int. Ed.*, vol. 64, no. 4, 2023, doi: https://doi.org/10.1002/anie.202215947.

[26] P. Tiwari *et al.*, "Design and Simulation of Efficient SnS-Based Solar Cell Using Spiro-OMeTAD as Hole Transport Layer," *Nanomaterials*, vol. 12, no. 14, pp. 1–9, 2022, doi: 10.3390/nano12142506.

[27] M. Serhan *et al.*, "Interface Engineering for High-Performance Perovskite Hybrid Solar Cells," *J. Mater. Chem. A*, vol. 3, pp. 19205–19217, 2015, doi: 10.1039/x0xx00000x.

[28] N. G. Materials and B. M. Studio, "BIOVIA MATERIALS STUDIO OVERVIEW".

[29] S. J. Clark, M. D. S. Ii, C. J. P. Ii, P. J. H. Iii, M. I. J. P. Iv, and K. R. V, "First principles methods using CASTEP," vol. 220, pp. 567–570, 2005.

[30] S. C. Mouna, "ETUDE DES PROPRIETES OPTOELECTRIQUE D'UN MATERIAU TCO EN COUCHES MINCES APPLICATION: CONVERSION PHOTOVOLTAIQUE," 2017.

[31] E. V V.MILMAN, B.WINKLER, Akhmatskaya and R. H. Nobes, "Phase Stability of Inorganic Crystals : A Pseudopotential Plane-Wave Study," *Int. J. Quantum Chem.*, vol. 77, no. 2000, pp. 895–910, 1999, [Online]. Available: http://onlinelibrary.wiley.com/doi/10.1002/(SICI)1097-461X(2000)77:5%3C895::AID-QUA10%3E3.0.CO;2-C/abstract

[32] M. Burgelman, K. Decock, A. Niemegeers, J. Verschraegen, and S. Degrave, "SCAPS

manual," 2023.

[33] O. Ourahmoun, "Les cellules solaires à base de matériaux pérovskites - Structures et performances," vol. 21, pp. 515–520, 2018.

[34] F. Anwar, R. Mahbub, S. S. Satter, and S. M. Ullah, "Research Article Effect of Different HTM Layers and Electrical Parameters on ZnO Nanorod-Based Lead-Free Perovskite Solar Cell for High-Efficiency Performance," no. November, 2017, doi: 10.1155/2017/9846310.

[35] Y. H. Joo, D. S. Um, and C. Il Kim, "Tunable physical properties of Al-doped ZnO thin films by O2and Ar plasma treatments," *Mater. Res. Express*, vol. 8, no. 12, pp. 0–9, 2021, doi: 10.1088/2053-1591/ac3f0a.

[36] E. N. Vincent Mercy, D. Srinivasan, and L. Marasamy, "Emerging BaZrS3 and Ba(Zr,Ti)S3 Chalcogenide Perovskite Solar Cells: A Numerical Approach Toward Device Engineering and Unlocking Efficiency," *ACS Omega*, vol. 4, pp. 4359–4376, 2024, doi: 10.1021/acsomega.3c06627.

[37] L. Luo *et al.*, "Study of Se/Te-doped Cu2O as a hole transport material in perovskite solar cells," *RSC Adv.*, vol. 13, no. 13, pp. 8476–8486, Mar. 2023, doi: 10.1039/D2RA04659H.

[38] S. C. Mouna, M. Radjai, A. Rahman, A. Bouhemadou, D. Houatis, and D. Allali, "Physical properties of Be-based fluoroperovskite compounds XBeF 3 (X = K , Rb): a first-principles study," vol. 36, 2024.

[39] Y. Nassah *et al.*, "Electronic band structure , mechanical and optical characteristics of new lead-free halide perovskites for solar cell applications based on DFT computation," *Bull. Mater. Sci.*, vol. 0123456789, 2023, doi: 10.1007/s12034-023-02890-x.